

# Syntheses, Crystal Structure, Electrocatalytic, and Magnetic Properties of the Monolanthanide-Containing Germanotungstates $[\text{Ln}(\text{H}_2\text{O})_n\text{GeW}_{11}\text{O}_{39}]^{5-}$ ( $\text{Ln} = \text{Dy}, \text{Er}, n = 4, 3$ )

Masooma Ibrahim,<sup>\*,†</sup> Israël M. Mbomekallé,<sup>‡</sup> Pedro de Oliveira,<sup>‡</sup> Ananya Bakshi,<sup>†</sup> Anthony B. Carter,<sup>§,||</sup> Yan Peng,<sup>§</sup> Thomas Bergfeldt,<sup>⊥</sup> Sharali Malik,<sup>†</sup> and Christopher E. Anson<sup>§</sup>

<sup>†</sup>Institute of Nanotechnology, Karlsruhe Institute of Technology, Hermann von-Helmholtz Platz 1, 76344 Eggenstein-Leopoldshafen, Germany

<sup>‡</sup>Equipe d'Electrochimie et Photo-électrochimie, Laboratoire de Chimie Physique, Université Paris-Sud, UMR 8000, CNRS-Université Paris Saclay, Orsay F-91405, France

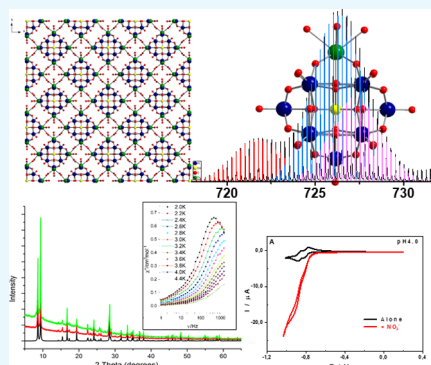
<sup>§</sup>Institute of Inorganic Chemistry, Karlsruhe Institute of Technology, Engesserstrasse 15, 76128 Karlsruhe, Germany

<sup>||</sup>School of Chemistry University of Southampton University Road, SO17 1BJ Southampton, U.K.

<sup>⊥</sup>Institutes for Applied Materials (IAM-AWP), Karlsruhe Institute of Technology (KIT), 76131 Karlsruhe, Germany

## Supporting Information

**ABSTRACT:** Two monolanthanide-containing polyanions based on monolacunary Keggin germanotungstates  $[\text{Ln}(\text{H}_2\text{O})_n\text{GeW}_{11}\text{O}_{39}]^{5-}$  ( $\text{Ln} = \text{Dy}, \text{Er}, n = 4, 3$ ) have been synthesized in simple one-pot synthetic procedure and compositionally characterized in solid state by single-crystal X-ray diffraction, powder X-ray diffraction, Fourier transform infrared spectroscopy, thermogravimetric analysis, and elemental analysis. Electronic absorption and emission spectra of the title compounds in solution were also studied. The  $[\text{Dy}^{\text{III}}(\text{H}_2\text{O})_4\text{GeW}_{11}\text{O}_{39}]^{5-}$  Keggin POM exhibits a slow relaxation of magnetization. The cyclic voltammetry measurements and mass spectrometry were carried out to check the stability of the compounds in solution. Both polyanions prove efficient in the electrocatalytic reduction of nitrite. To our knowledge, this observation establishes the first example of electrocatalysis of nitrite reduction by all inorganic monolanthanide-containing germanotungstates family.



## INTRODUCTION

Polyoxometalates (POMs) are discrete metal oxygen cluster anions constructed from early transition metals ( $M = \text{V}, \text{Nb}, \text{Ta}, \text{Mo}, \text{W}$ ) in their highest oxidation state and are being extensively studied because of their application in catalysis, energy, molecular magnetism, biochemistry, optics, and separation science.<sup>1–16</sup> Lacunary POM ligands are versatile inorganic building blocks for the construction of molecule-based materials. However, the reaction conditions such as concentration of the reactants, temperature, pH value, time, pressure, and organic/inorganic co-ligands can also play an important role in the isolation of desired products. Meanwhile, the structural varieties and functionalities of these materials could be tuned by the incorporation of different transition-metal ions,<sup>17–20</sup> rare earth (RE) metal cations,<sup>21–27</sup> and mixed TM–RE metal centers.<sup>28–31</sup> Lanthanide cations with high coordination number are generally considered as suitable linkers for linking POM fragments into discrete nanosized POM frameworks or extended structures. In other words, the larger ionic size of 4f ions compared to 3d metal ions hinder their full incorporation in the lacunary sites of the POM

ligands; therefore, additional sites are available for further derivatization, which result in giant architectures.<sup>32–45</sup>

Over the last few decades, lanthanide-containing POMs (LnPOMs) have been mainly studied because of their potential applications in various fields, such as molecular magnetism,<sup>3,10,46</sup> photoluminescence,<sup>4,47–49</sup> and imaging.<sup>50,51</sup> In the field of molecular magnetism, lanthanide ions (typically Tb, Dy, Ho, and Er) are investigated for the search of single-molecule magnets (SMMs) with a high blocking temperature due to their usual large magnetic moments and large magnetic anisotropy. Single-molecule magnets are individual high-spin molecules displaying a slow spin relaxation and preserving their magnetic moment below the characteristic blocking temperature ( $T_B$ ).<sup>3,10,46</sup> Interestingly,  $[\text{ErW}_{10}\text{O}_{36}]^{9-}$  is the first polyoxometalate behaving as a single-molecule magnet (SMM) and can be considered as a molecular analogue of classical bulk ferromagnet.<sup>46</sup> Regarding the advances of POMs in catalysis, the most fascinating properties of POMs in the

Received: September 3, 2019

Accepted: November 18, 2019

Published: December 10, 2019

catalysis applications are their high thermal stability, structural flexibility, tunable redox potential, and fundamental impedance to oxidative decomposition. These unique properties allow the POMs-based catalysts to be constructed at the molecular level. The catalytically active sites of POMs can be finely tuned with an appropriate combination of lanthanide cation and lacunary POMs as inorganic ligands. Numerous LnPOM catalysts have been produced with different structural types (i.e., Keggin versus Dawson) and chemical compositions (nature and number of rare earth metals incorporated). The concurrence of both Lewis acid (Ln ions) and Lewis base (POM) in LnPOMs has been found to show great potential in the development of catalytic systems for various chemical processes and various organic reactions.<sup>52–58</sup> The first report on monolanthanide-containing POMs were published in 1971 by Peacock and Weakley, which showed that lanthanide cations react rapidly with monolacunary  $[\alpha\text{-SiW}_{11}\text{O}_{39}]^{8-}$  to give both 1:1 and 1:2 LnPOMs.<sup>59</sup> Some examples of 1:1 LnPOM are  $[\text{RE}(\text{H}_2\text{O})_n(\text{XW}_{11}\text{O}_{39})]^{m-}$  (X = Si, Ge, P, RE = La<sup>III</sup>, Ce<sup>III</sup>, Nd<sup>III</sup>, Sm<sup>III</sup>, Eu<sup>III</sup>, Yb<sup>III</sup>, Gd<sup>III</sup>, Dy<sup>III</sup>, Y<sup>III</sup>) and  $[\text{Ln}(\alpha\text{-SiW}_{11}\text{O}_{39})(\text{H}_2\text{O})_3]^{5-}$  (Ln = La<sup>III</sup>, Pr<sup>III</sup>, Ce<sup>III</sup>, Nd<sup>III</sup>, Sm<sup>III</sup>, Eu<sup>III</sup>, Yb<sup>III</sup>, Gd<sup>III</sup>), and examples of 1:2 LnPOM are  $[\text{Ln}(\alpha\text{-SiW}_{11}\text{O}_{39})_2]^{13-}$  (Ln = Nd<sup>III</sup>, Pr<sup>III</sup>, Ce<sup>III</sup>).<sup>27,60–67</sup>

Kortz and co-workers reported the synthesis and structural characterization of dimeric 1:2 LnPOMs  $[\text{Ln}(\beta_2\text{-SiW}_{11}\text{O}_{39})_2]^{13-}$  (Ln = La<sup>III</sup>, Ce<sup>III</sup>, Sm<sup>III</sup>, Eu<sup>III</sup>, Gd<sup>III</sup>, Tb<sup>III</sup>, Yb<sup>III</sup>, Lu<sup>III</sup>) based on chiral Keggin units  $[\beta_2\text{-SiW}_{11}\text{O}_{39}]^{8-}$ .<sup>68</sup> Zhang et al. studied the static electrostatic interactions of the gadolinium derivative  $[\text{Gd}(\beta_2\text{-SiW}_{11}\text{O}_{39})_2]^{13-}$  with human serum albumin.<sup>69</sup> There are many reports on organic–inorganic hybrid monolacunary Keggin polyoxotungstate based 3d–4f heterometallic derivatives where  $[\text{RE}(\text{H}_2\text{O})_n(\text{XW}_{11}\text{O}_{39})]^{m-}$  and copper–organic linkers have been used to make extended architectures.<sup>70–84</sup> Here, we report on the monolanthanide-containing polyanions based on the monolacunary  $\alpha$ -Keggin tungstogermanate,  $[\text{Ln}(\text{H}_2\text{O})_n(\text{GeW}_{11}\text{O}_{39})]^{5-}$  (Ln = Dy, Er,  $n = 4, 3$ ), which have been synthesized under normal bench conditions by the reaction of  $\text{LnCl}_3 \cdot 6\text{H}_2\text{O}$  (Ln = Dy, Er) and  $\text{K}_8[\gamma\text{-GeW}_{10}\text{O}_{36}] \cdot 6\text{H}_2\text{O}$  in 1 M LiOAc buffer pH 4.8 and characterized by single-crystal X-ray crystallography, powder X-ray diffraction, Fourier transform infrared spectroscopy, elemental analysis, thermogravimetric analysis, mass spectrometry, UV–vis absorption spectroscopy, and luminescence spectroscopy. The solution-stable title compounds were tested for their activity in the electrocatalytic reduction of nitrite.

## RESULTS AND DISCUSSION

**Synthesis.** The title polyanions  $[\text{Dy}(\text{H}_2\text{O})_4\text{GeW}_{11}\text{O}_{39}]^{5-}$  (**1**) and  $[\text{Er}(\text{H}_2\text{O})_3\text{GeW}_{11}\text{O}_{39}]^{5-}$  (**2**) were prepared by the reaction of Ln<sup>III</sup> (Ln = Dy, Er) ions with dilacunary Keggin-type polyanion  $[\gamma\text{-GeW}_{10}\text{O}_{36}]^{8-}$  in 1 M LiOAc buffer (pH 4.8) media at 70 °C. It is important to note that the isolation of  $\text{K}_5[\text{Dy}(\text{H}_2\text{O})_4\text{GeW}_{11}\text{O}_{39}] \cdot 16\text{H}_2\text{O}$  (**K-1**) and  $\text{K}_5[\text{Er}(\text{H}_2\text{O})_3\text{GeW}_{11}\text{O}_{39}] \cdot 20\text{H}_2\text{O}$  (**K-2**) was only possible at pH 4.8 and with metastable precursor polyanion  $[\gamma\text{-GeW}_{10}\text{O}_{36}]^{8-}$ . The morphology of the isolated POM crystals were investigated by scanning electron microscopy (SEM). Figure 12 shows the micrographs of **K-1** and **K-2**, which have tetragonal crystals and rectangular block crystals, respectively.

**Single-Crystal X-Ray Structure Determination.** The molecular and packing structures of  $[\text{Dy}(\text{H}_2\text{O})_4\text{GeW}_{11}\text{O}_{39}]^{5-}$  (**1**) and  $[\text{Er}(\text{H}_2\text{O})_3\text{GeW}_{11}\text{O}_{39}]^{5-}$  (**2**) were determined by

single-crystal X-ray diffraction (Figures 1, 2, 3). Since the two monolanthanide-substituted Keggin-type polyoxotungstates **K-**

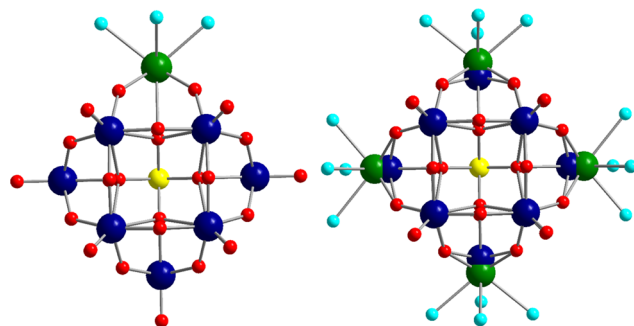


**Figure 1.** Ball-and-stick representation of the  $[\text{Dy}(\text{H}_2\text{O})_4\text{GeW}_{11}\text{O}_{39}]^{5-}$  anion. Color scheme: Dy = green; O = red; aqua ligand = turquoise; W = dark blue, Ge = yellow. Left: molecular structure. Right: Structure showing the 1:3 Dy/W disorder over four crystallographically equivalent sites and the 2-fold oxygen disorder about Ge(1).

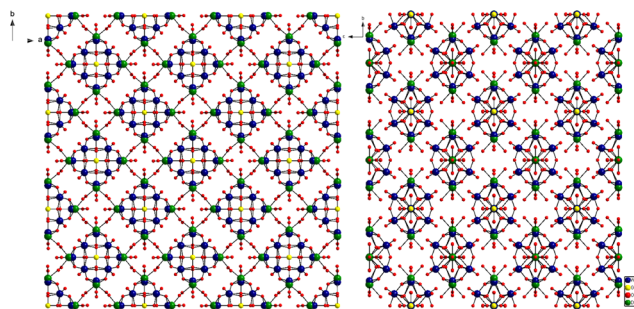


**Figure 2.** Ball-and-stick representation of the crystal packing arrangement for  $[\text{Dy}(\text{H}_2\text{O})_4\text{GeW}_{11}\text{O}_{39}]^{5-}$ . Right: along the  $a$ -direction. Left: along the  $c$ -direction. Color scheme: Dy = green; O = red; W = dark blue, Ge = yellow. K cations are omitted for clarity.

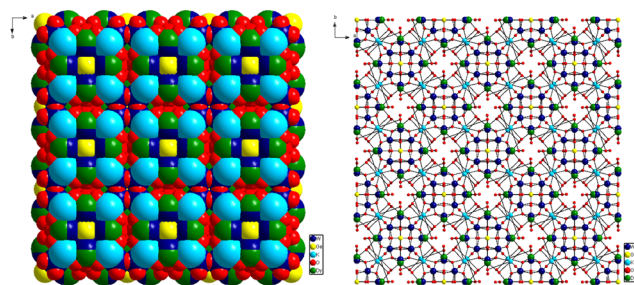


**Figure 3.** Right: ball-and-stick representation of the crystal packing arrangement along the  $c$ -direction for  $[\text{Dy}(\text{H}_2\text{O})_4\text{GeW}_{11}\text{O}_{39}]^{5-}$ . Left: space filled representation of the crystal packing arrangement along the  $c$ -direction for  $[\text{Dy}(\text{H}_2\text{O})_4\text{GeW}_{11}\text{O}_{39}]^{5-}$ . Color scheme: Dy = green; O = red; W = dark blue; Ge = yellow; K = light blue.

**1** and **K-2** are crystallized as isomorphous potassium salts in the tetragonal space group  $I4/m$  with  $Z = 2$ , only the crystal structure of **K-1** will be described. Both polyanions belong to the 1:1 class of LnPOMs based on monolacunary Keggin ions. The compound **1** is similar to  $[\text{Dy}(\text{H}_2\text{O})_2(\text{GeW}_{11}\text{O}_{39})]^{5-}$  reported by group of Yang.<sup>60</sup> The molecular structure of the  $[\text{Dy}(\text{H}_2\text{O})_4\text{GeW}_{11}\text{O}_{39}]^{5-}$  anion is based on that of the Keggin  $[\text{GeW}_{12}\text{O}_{40}]^{4-}$  anion, but with one of the four W = O residues lying on the  $I4/m$  mirror plane replaced by a  $\{\text{Dy}(\text{OH})_2\}^{3+}$  moiety. Since  $\text{Dy}(2\text{B})\text{-O}(1)$ , where O(1) is the germanate

oxygen, is over 2.8 Å, the Dy<sup>III</sup> cation is best described as eight-coordinated with a square-antiprismatic geometry. The structural analysis shows that **K-1** forms an unusual closed three-dimensional (3D) framework architecture. Four K<sup>+</sup> per cluster link the polyoxometalates into a 3D structure; the fifth K<sup>+</sup> occupies the only available lattice cavity in the structure, leaving no space for any lattice waters within the crystal structure. The Er analogue **K-2** differs only in the number of aqua ligands coordinated to Er(2B); from the thermal parameters of these, it is likely that there are only three such ligands in the Er compound, consistent with the smaller ionic radius of Er<sup>III</sup>. The aqua ligand variation in isostructural compounds **K-1** and **K-2** demonstrates that the lanthanide contraction effect can play a prominent role in the coordination environment of the lanthanide cations.<sup>85</sup> To the best of our knowledge, this represents a rare all-inorganic 3D framework based on the monolanthanide-substituted Keggin tungstogermanate. The Keggin fragments are of  $\alpha$ -type in polyanions **1** and **2**. The conversion of polyanion precursor from  $[\gamma\text{-GeW}_{10}\text{O}_{36}]^{8-}$  to  $[\alpha\text{-GeW}_{11}\text{O}_{39}]^{8-}$  in acidic media have been facilitated by the presence of lanthanide ions in the reaction mixture. Previously, such a conversion has been observed under the hydrothermal condition by the Yang group.<sup>86</sup> Polyoxoanion **1** contains one  $[\alpha\text{-GeW}_{11}\text{O}_{39}]^{8-}$  subunit and one dysprosium metal ion, which occupies the position that has been created by removal of a W–O<sub>t</sub> group from the  $[\alpha\text{-GeW}_{12}\text{O}_{40}]^{4-}$  anion, which consists of a central {GeO<sub>4</sub>} tetrahedron surrounded by four vertex-sharing {W<sub>3</sub>O<sub>13</sub>} triads. Polyanion  $[\text{Dy}(\text{H}_2\text{O})_4\text{GeW}_{11}\text{O}_{39}]^{5-}$  is surrounded by potassium as a counter cation, which is coordinated by eight O atoms. It should be noted that both structures have substitutional disorder of Ln/W in the Keggin anion, which has been refined with a Ln/W site occupancy ratio of 0.25:0.75. It is a well-known fact that the structures of most metal-substituted Keggin derivatives are disordered as a result of the high symmetry of the Keggin ion.<sup>87</sup> It is important to mention that the dilacunary polyanion  $[\gamma\text{-GeW}_{10}\text{O}_{36}]^{8-}$  can easily isomerize and/or decompose in acidic aqueous solutions to the corresponding  $\alpha$ - and  $\beta$ -isomers due to its metastable nature in solution state. Normally, dilacunary  $\alpha$ -Keggin fragments have a strong tendency to transform to either  $[\alpha\text{-GeW}_{11}\text{O}_{39}]^{8-}$  or plenary Keggin ion  $[\alpha\text{-GeW}_{12}\text{O}_{40}]^{4-}$  by uptaking additional W<sup>VI</sup> centers (which can form in solution by partial decomposition of the POM precursor) in acidic media below pH 5. However, the trilacunary derivative  $[\alpha\text{-GeW}_9\text{O}_{34}]^{10-}$  anions are formed from the partial base degradation of Keggin anions by the loss of a tungsten atom.<sup>84,88,89</sup> Interestingly, transition-metal-substituted Keggin polyanions, which could lead to the different multidimensional structures, are currently investigated in the field of molecular magnetism<sup>90</sup> and hydrogen evolution catalysis.<sup>87</sup> These lanthanide-containing Keggin-type structures ( $[\text{Ln}(\text{H}_2\text{O})_n\text{GeW}_{11}\text{O}_{39}]^{5-}$  (Ln = Dy, Er,  $n = 4,3$ )) have potential to be used as functional building block units for the formation of porous nanostructured with the interaction of large cations i.e.,  $[\text{M}_3\text{O}(\text{OAc})_6(\text{CH}_3\text{OH})_3]^+$  (M = Ru, Cr) and Ln<sup>III</sup> cations as linkers. This synthetic approach has been recently investigated, where the combination of large cations with symmetrical Keggin-type anions {GeW<sub>12</sub>} and {SiMo<sub>12</sub>} led to the formation of novel materials with functionalities that can reflect both cationic and anionic moieties.<sup>11,91–93</sup> Trials to obtain analogues of **1** and **2** with other lanthanide cations are currently underway.

**PXRD Analyses.** Powder X-ray diffraction (PXRD) is one of the most useful tools to check the bulk purity of the crystalline solids. PXRD was used to confirm the identity and phase purity of crystallines **K-1** and **K-2**. The measured powder pattern and the simulated pattern from the solved crystal structure match perfectly, which is a sufficient proof of phase-pure compounds (Figure 4).

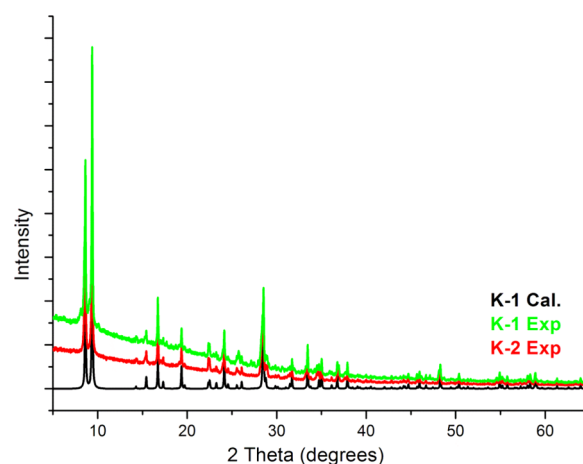


**Figure 4.** Experimental diffraction powder patterns of **K-1** and **K-2** and the calculated diffraction powder pattern from the single-crystal X-ray diffraction structure of **K-1**.

**IR Spectroscopy.** Infrared spectroscopy is another frequently employed technique for the characterization of polyoxometalates due to their characteristic peaks in the region (1200–450 cm<sup>-1</sup>), which is called the fingerprint region for the POM skeleton. The difference/shift in the characteristic bands of the lacunary precursor  $\text{K}_8[\gamma\text{-GeW}_{10}\text{O}_{36}] \cdot 6\text{H}_2\text{O}$  and synthesized compounds indicate the formation of new compounds. Further, the similarity in the Fourier transform infrared (FTIR) spectra of **K-1** and **K-2** exhibit the isostructural nature of the compounds (Figure S1).

**TG Analyses.** Thermogravimetric (TG) analyses were carried out to examine the thermal stability of **K-1** and **K-2** in solid state and the total content of water molecules in the bulk material. In line with the structural similarity of **K-1** and **K-2**, quite similar thermograms are observed for both. The TG curves of **K-1** and **K-2** in the range of room temperature to 1000 °C exhibit a gradual weight loss step up to ca. 640 °C, which correspond to the removal of the surface-adsorbed water molecules and crystal waters as well (Figure S3). The total amount of water estimated by thermogravimetric analysis was clearly higher than those obtained by the single-crystal structure analysis. This is due to the difference in the single-crystal sample and bulk sample that contain surface-adsorbed water molecules. The overall elemental composition of the bulk material was also determined by complete elemental analysis. Thus, for bulk studies, the compounds were formulated as  $\text{K}_5[\text{Dy}(\text{H}_2\text{O})_4\text{GeW}_{11}\text{O}_{39}] \cdot 16\text{H}_2\text{O}$  (**K-1**) and  $\text{K}_5[\text{Er}(\text{H}_2\text{O})_3\text{GeW}_{11}\text{O}_{39}] \cdot 20\text{H}_2\text{O}$  (**K-2**) based on single-crystal X-ray crystallography, elemental analysis, and thermogravimetric analysis.

**UV–vis Spectroscopy.** UV–vis spectroscopy measurements were performed on polyanions **K-1** and **K-2**, and compared with the absorption spectrum of  $\text{K}_8[\alpha\text{-GeW}_{11}\text{O}_{39}] \cdot 13\text{H}_2\text{O}$ . As shown in Figure S4, two strong absorption bands with maximum around 200 and 250 nm are observed in the

spectra of **1** and **2** solutions. The peak at 200 nm is attributed to the  $O_d \rightarrow W$  charge transition and the other peak at 250 nm is assigned to the  $O_{b(c)} \rightarrow W$  charge transition. These dominant ligand-to-metal charge-transfer bands are the two characteristic bands of Keggin heteropolytungstate complexes, which appear due to the transfer of electrons from filled oxygen orbitals to the empty 5d orbitals of the  $W^{VI}$  ions. However, the absorption peaks in **1** and **2** have an obvious blue shift, and the intensity is enhanced compared to that of the  $[\alpha\text{-GeW}_{11}\text{O}_{39}]^{8-}$ , which confirms the combination of  $[\alpha\text{-GeW}_{11}\text{O}_{39}]^{8-}$  and Ln ions (Ln = Dy, Er).

**Emission Spectroscopy.** Room-temperature photoluminescence experiments were performed on **K-1**, **K-2**, and  $K_8[\alpha\text{-GeW}_{11}\text{O}_{39}] \cdot 13\text{H}_2\text{O}$  in aqueous solution. When the emission spectra of **K-1**, **K-2**, and  $K_8[\alpha\text{-GeW}_{11}\text{O}_{39}] \cdot 13\text{H}_2\text{O}$  were studied with excitation at 250 nm, the clearly visible peaks at 350, 550, and 667 nm were observed. The same behavior was observed when the molecules were irradiated with 300 nm excitation wavelengths. As depicted in Figure S5, the emission spectra of **K-1**, **K-2**, and  $K_8[\alpha\text{-GeW}_{11}\text{O}_{39}] \cdot 13\text{H}_2\text{O}$  are, apart from intensity, almost the same at room temperature, where the tungstogermanate emission is quenched. It can also be observed that the emission intensity varied slightly from **K-1** to **K-2**. The resultant similar emission profiles, but with different intensities, suggest the well-known quenching effect of water molecules on the luminescence of POMs. This condensation of tungstate groups results in more efficient emission; therefore, the luminescence of the  $\{\text{GeW}_{11}\}$  is not unexpected. However the coordination environment and electronic nature of the incorporated metal ions also determines the luminescence efficiency.<sup>4,94</sup> From these structural arguments, it becomes clear that both **K-1** and **K-2** exhibited tungstate emission instead of a  $\text{Ln}^{III}$  emission.

**Mass Spectrometry.** Mass spectrometry (MS), specifically electrospray ionization (ESI) MS, has been found to be useful in determining the intact POMs core as they generally possess high inherent negative charge. In this work, high-resolution ESI MS was used in water and acetonitrile mixture. Intact cluster ion for both compounds **K-1** and **K-2** was observed in ESI MS in the negative-ion mode. Strong signal with a single cation was observed for a 4-anionic cluster with various number of attached  $\text{H}_2\text{O}$  molecules. For **K-1**, Li-exchanged peak appeared at the maximum intensity at  $m/z$  722.2 and 726.8, which are assigned as  $\text{Li}[\text{DyGeW}_{11}\text{O}_{39}]^{4-}$  and  $\text{Li}[\text{Dy}(\text{H}_2\text{O})\text{GeW}_{11}\text{O}_{39}]^{4-}$ , respectively. Broad mass envelope compared with several possible metal-ion exchanges is shown in Figure 5. Protonated and sodiated peaks were seen with lower intensity, suggesting higher stability with Li exchange compared to H or Na. Several K-exchanged peaks were also seen. Corresponding 3-charged ions were seen in the mass range  $m/z$  960–1030. Plausible assignments are given in Table S1. Several dimeric and trimeric peaks with a higher charge (5) were also seen in the higher mass range ( $m/z$  1200–2000), confirming bonded stable structural motifs even in the gas phase.

Similar ions were found when **K-2** was analyzed following similar experimental condition. In case of **K-2**, protonated  $\text{H}[\text{ErGeW}_{11}\text{O}_{39}]^{4-}$  and  $\text{H}[\text{Er}(\text{H}_2\text{O})\text{GeW}_{11}\text{O}_{39}]^{4-}$  were found at maximum intensity unlike that of **K-1**. Li exchange peak, although merged with the next peak, is visible as shown in Figure 6 (inset i). Although Na exchange peak  $\text{Na}[\text{ErGeW}_{11}\text{O}_{39}]^{4-}$  contributes to the similar mass range of  $\text{Na}[\text{Er}(\text{H}_2\text{O})\text{GeW}_{11}\text{O}_{39}]^{4-}$ , it was identifiable when compared with the calculated isotope pattern. Corresponding 3-species

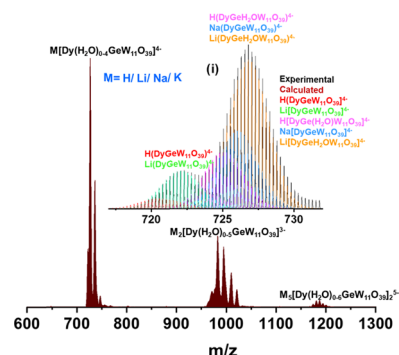


**Figure 5.** ESI MS of **K-1** showing 2 sets of peaks at the mass range 710–760 and 960–1030 corresponding to 4- and 3-charge state, respectively. Strongest peak at  $m/z$  715–730 is expanded in the inset (i). Different alkali-metal-exchanged peaks were observed and the mass envelope is compared with 5 different possible compositions, and their calculated isotope distribution pattern is overlaid.

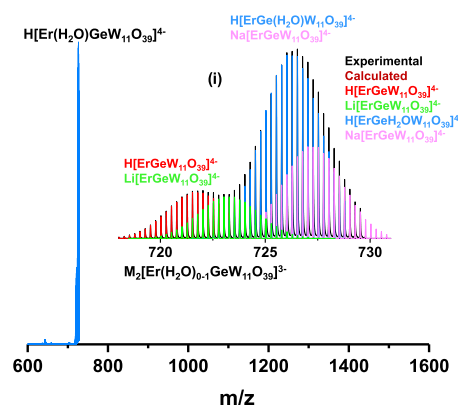


**Figure 6.** ESI MS of **K-2** shows 2 sets of peaks at the mass range 710–760 and 960–1030 corresponding to 4- and 3-charge states, respectively. Strongest peak at  $m/z$  715–730 is expanded in the inset (i). Different alkali-metal-exchange peaks are observed and the mass envelope is compared with 4 different possible compositions, and their calculated isotope distribution pattern is overlaid.

was observed in the mass range  $m/z$  960–1030. The source of Li ions, which have been identified by mass spectrometry, is the adsorption of mother liquor (1 M LiAcO buffer solution) at the crystal surface. However, the source of Na ion is not clear.

**Electrochemical Characterization.** The two compounds **K-1** and **K-2** seem to be sufficiently stable in lithium acetate medium, in which they were synthesized, to be characterized by cyclic voltammetry (CV). Upon comparing the CV of POM **2** with that of  $\{\text{GeW}_{11}\}$  at pH 4 (Figure 7A), there is a shift of the redox peak potentials toward less negative values when  $\{\text{GeW}_{11}\}$  is coordinated with Er cation. In fact, the main peak of the wave attributed to the reduction of  $W(VI)$  centers was measured at  $-0.91$  V vs saturated calomel electrode (SCE) from the CV of  $\{\text{GeW}_{11}\}$  and at  $-0.89$  V vs SCE from the CV of polyanion **2**. The composite feature of the same reduction wave is more obvious in the case of compound **2**, which has a clear shoulder at  $-0.82$  V vs SCE, indicative of a more pronounced alkaline character for this Er-substituted species when compared to  $\{\text{GeW}_{11}\}$ .<sup>95</sup> Figure S6 shows the CVs of the two compounds recorded at different scan rates (ranging from 10 to 100  $\text{mVs}^{-1}$ ) and the linear dependency of the peak current on the square root of the scan rate, revealing that the

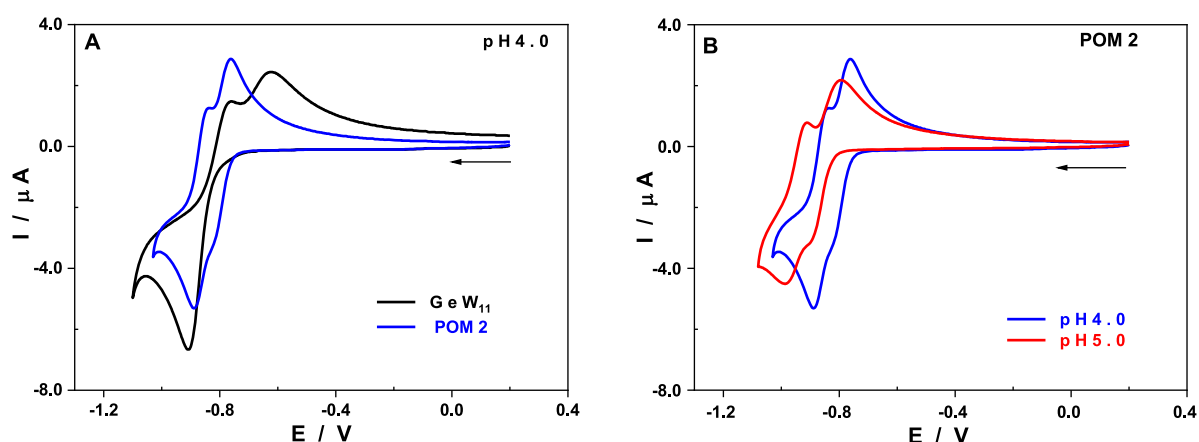


**Figure 7.** (A) CVs of {GeW<sub>11</sub>} (black) and POM 2 (blue) recorded in 1.0 M LiCH<sub>3</sub>CO<sub>2</sub> + CH<sub>3</sub>CO<sub>2</sub>H/pH 4.0. (B) CVs of POM 2 recorded in 1.0 M LiCH<sub>3</sub>CO<sub>2</sub> + CH<sub>3</sub>CO<sub>2</sub>H/pH 4.0 (blue) and in pH 5.0 (red). POM concentration: 0.50 mM. Working electrode: EPG; counter electrode: Pt gauze; reference electrode: SCE. Scan rate: 10 mVs<sup>-1</sup>.

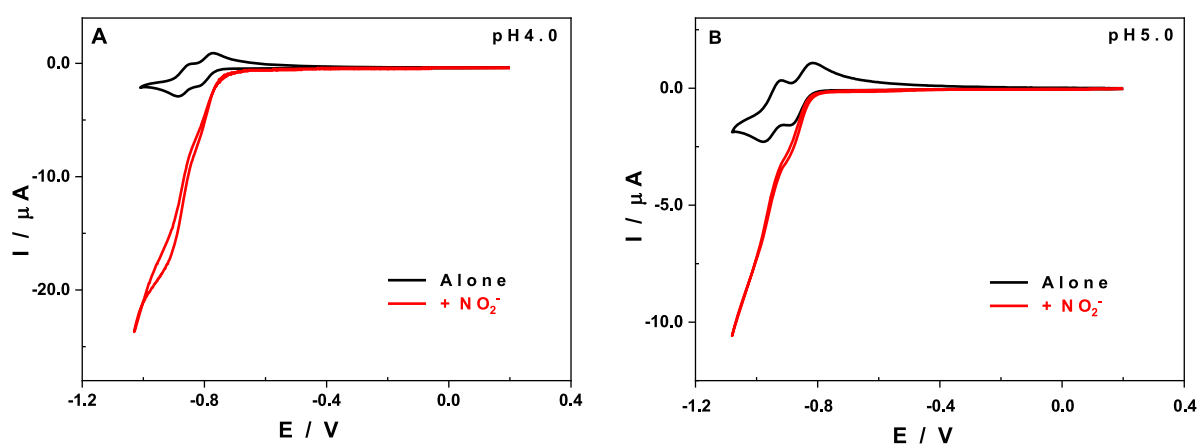


**Figure 8.** CVs of POM 2 recorded in 1.0 M LiCH<sub>3</sub>CO<sub>2</sub> + CH<sub>3</sub>CO<sub>2</sub>H in the absence (black) and presence (red) of nitrite ion (5.0 mM). (A) pH 4.0 and (B) pH 5.0. POM concentration: 0.50 mM. Working electrode: EPG; counter electrode: Pt gauze; reference electrode: SCE. Scan rate: 2 mVs<sup>-1</sup>.

electron-transfer process is entirely diffusion-controlled. Interestingly, this seems not to be the case with the compound Dy-GeW<sub>11</sub>. The CVs of POM 2 and of POM 1 exhibit marked similarities (Figure S7A); however, in the case of the latter, there is a decrease of the peak current upon successive cycling. This behavior suggests the formation of a film that influences the response of the electroactive surface of the working electrode (Figure S7B).

When the experiments are carried out at pH 5, the whole CVs shift toward the negative side of the potential scale (Figure 7B). In addition, the distinction between the two reduction steps becomes more evident, with a first peak at -0.90 V vs SCE, followed by a second one at -0.99 V vs SCE for Er-GeW<sub>11</sub>. At pH 5, the CVs of 2 and of 1 exhibit the same features and are strictly superimposable (Figure S8). The reduction of Ln cations present in tungstic POMs is difficult to observe in an aqueous medium. It generally takes place at very low potentials beyond the electrolyte reduction (water reduction wave). The reduction of Eu<sup>III</sup> centers has been demonstrated in several cases because this cation is reduced at the same potential range as the W<sup>VI</sup> centers, but the other Ln cations are expected to remain electrochemically silent in our experimental conditions.<sup>96–98</sup>

**Electrocatalytic Properties.** The electrocatalytic properties of POM 2, which is representative of the two compounds, have also been studied. In the presence of an excess nitrite ions, the CVs of compound 2 undergo notable changes, namely, the loss of reversibility of the reduction waves (Figures 8 and S9), indicative of the existence of an electrocatalytic phenomenon. The latter becomes more pronounced when the CVs are recorded at small scan rates. This effect may be quantified by the catalytic current,  $I_{CAT}$ , which was calculated for each scan rate at a convenient potential value, corresponding to the peak potential of the reduction wave in the absence of nitrite ions:  $I_{CAT} = [(i_x - i_0)/i_0] \times 100$ , with  $i_x$  and  $i_0$  being the peak currents in the presence and in the absence of nitrite, respectively.<sup>99</sup> In both cases, that is at pH 4 and 5,  $I_{CAT}$  represents the catalytic efficiency of the POM toward the electroreduction of nitrite ions, which increases exponentially when the scan rate decreases (Figure 9). At pH 5,  $I_{CAT}$  varies from 15% at  $\nu = 100$  mVs<sup>-1</sup> to almost 200% at  $\nu = 2$  mVs<sup>-1</sup>. At pH 4, the effect is even more pronounced,  $I_{CAT}$  increases from 30% up to almost 500% within the same scan rate span.

**Magnetic Properties.** To explore the potential SMM behavior, alternating current (ac) magnetic susceptibility studies were carried out on freshly filtered samples of K-1

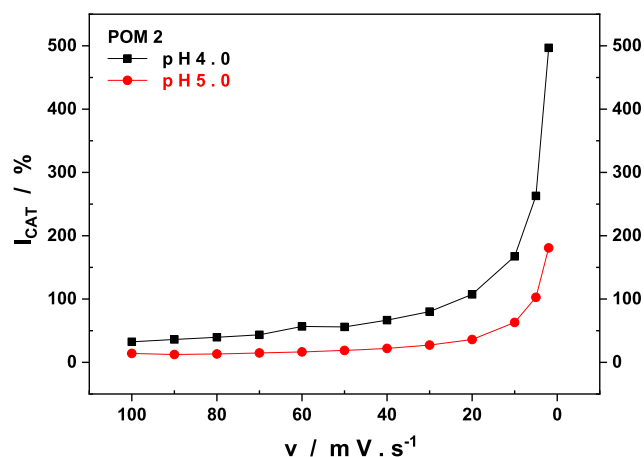


**Figure 9.** Evolution of the catalytic current,  $I_{\text{CAT}}$ , as a function of the scan rate,  $\nu$ , at pH 4.0 (black) and pH 5.0 (red).

compound. The ac signals were observed in the out of phase without the maxima, which is probably due to the presence of quantum tunneling of magnetization (QTM) (Figure 10). The

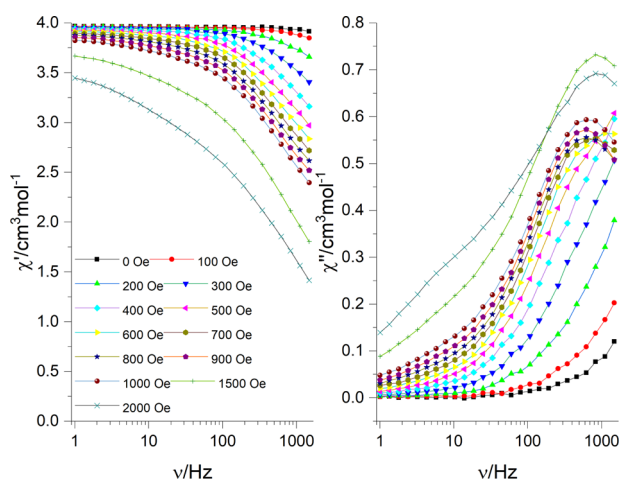


**Figure 10.** Plots of  $\chi'$  (left) and  $\chi''$  (right) vs frequency under different applied dc magnetic fields for K-1 at 2 K.

presence of QTM can reduce the expected energy barrier, but it is often possible to shortcut the QTM by applying a small static direct current (dc) field over the range 0–2000 Oe. Therefore, ac susceptibility measurements were performed at various dc fields to find an optimum field of 900 Oe to slow down the relaxation time by reducing or suppressing the quantum tunneling of magnetization (Figure 10). Therefore, the in-phase ( $\chi'$ ) and out-of-phase ( $\chi''$ ) ac susceptibilities as functions of frequency at various temperatures have been measured using an applied dc field of 900 Oe (Figure 11). The frequency-dependent out-of-phase susceptibility signals only show clear maxima between 2.0 and 2.6 K within the measurable frequency window and therefore cannot be analyzed with an Arrhenius fit. Additional magnetic measurements are planned to be performed on K-1 and K-2.

## CONCLUSIONS

We have prepared a 1:1 family of LnPOMs  $[\text{Ln}(\text{H}_2\text{O})_n\text{GeW}_{11}\text{O}_{39}]^{5-}$  ( $\text{Ln} = \text{Dy}, \text{Er}, n = 4, 3$ ) in simple one-pot synthetic procedure and characterized in solid as well as

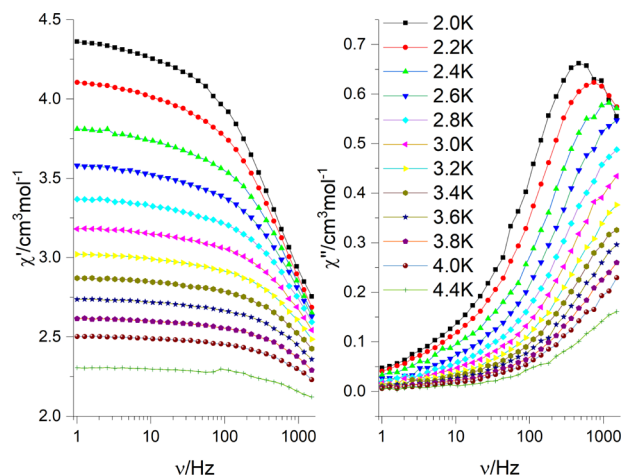


**Figure 11.** Plots of  $\chi'$  (left) and  $\chi''$  (right) vs frequency under 900 Oe dc magnetic fields for K-1 at different temperatures.

solution state. Both polyanions are formed by the transformation of the dilacunary POM precursor  $[\gamma\text{-GeW}_{10}\text{O}_{36}]^{8-}$  into the  $[\alpha\text{-GeW}_{11}\text{O}_{39}]^{8-}$  fragment in the presence of  $\text{Ln}^{\text{III}}$  ions, which led to the isolation of  $\{\text{LnGeW}_{11}\}$  1:1 LnPOMs. K-1 POM exhibits a slow relaxation of magnetization. Their stability in solution were evaluated by cyclic voltammetry and mass spectrometry. Both compounds show a strong catalytic activity towards the reduction of nitrite ions. This work shows that monolacunary polyanion fragments can be stabilized by lanthanide centers in solution and in the solid state. The isolated highly symmetrical LnPOM -Keggin must be ideal functional building blocks for the design of complex architectures.

## EXPERIMENTAL SECTION

The POM ligand,  $\text{K}_8[\gamma\text{-GeW}_{10}\text{O}_{36}] \cdot 6\text{H}_2\text{O}$ , was synthesized according to the literature methods and characterized by FTIR spectroscopy.<sup>100</sup> All reactions were carried out under aerobic conditions. All other reagents were purchased commercially and used without further purification.

**Synthetic Procedure for  $\text{K}_5[\text{Dy}(\text{H}_2\text{O})_4\text{GeW}_{11}\text{O}_{39}] \cdot 16\text{H}_2\text{O}$  (K-1).**  $\text{K}_8[\gamma\text{-GeW}_{10}\text{O}_{36}] \cdot 6\text{H}_2\text{O}$  (0.58 g, 0.20 mmol) was dissolved in 20 mL of 1 M lithium acetate buffer of pH 4.8. Then,  $\text{DyCl}_3 \cdot 6\text{H}_2\text{O}$  (0.23 g, 0.61 mmol) was added to this solution in small portions under stirring. The resultant turbid colorless solution was stirred and heated at 70 °C for one hour. Later, the solution was filtered and left to slowly evaporate at room temperature, and colorless crystals were obtained after approximately two weeks. Yield 19% (based on W). IR (2% KBr pellet,  $\nu/\text{cm}^{-1}$ ): 3421 (brd), 1622 (wk), 1563 (shp), 1462 (shp), 956 (shp), 884 (wk), 811 (wk) 678 (wk) 526, 464 (str), 401 (wk). Elemental analysis (%) calc<sup>-1</sup>d (found): K 5.69 (6.10), Dy 4.73 (4.73), W 58.83 (57.9), Ge 2.11 (2.03).

**Synthetic Procedure for  $\text{K}_5[\text{Er}(\text{H}_2\text{O})_3\text{GeW}_{11}\text{O}_{39}] \cdot 20\text{H}_2\text{O}$  (K-2).** The same procedure was employed to prepare (K-2) using  $\text{ErCl}_3 \cdot 6\text{H}_2\text{O}$  instead of  $\text{DyCl}_3 \cdot 6\text{H}_2\text{O}$ . Yield 20% (based on W). IR (2% KBr pellet,  $\nu/\text{cm}^{-1}$ ): 3423 (brd), 1623 (str) 1563 (shp), 1458 (shp), 956 (str), 885 (str), 813 (str), 679 (wk) 523 (wk) 466 (wk), 401 (wk). Elemental analysis (%) calcd (found): K 5.60 (5.52), Er 4.78 (4.92), W 57.85 (57.8), Ge 2.08 (2.00).

**Crystallography.** Data on single crystals of K-1 and K-2 were collected at 180 K on a Stoe IPDS II area detector

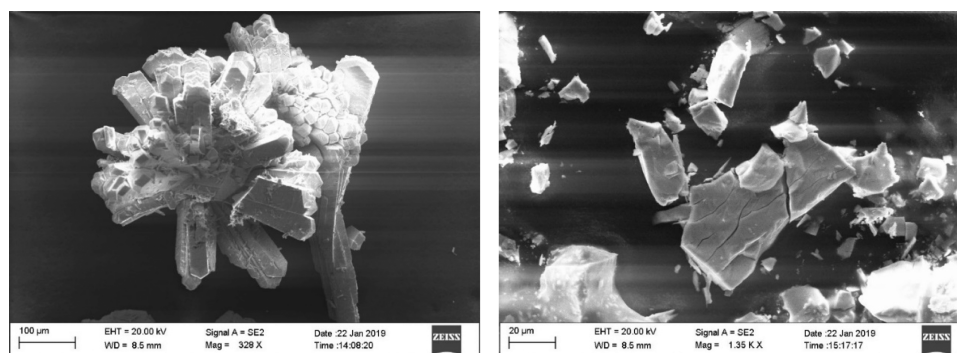


Figure 12. SEM images of (left) K-1 (right) K-2.

diffractometer using graphite-monochromated Mo  $K\alpha$  radiation (Table 1). Semiempirical absorption corrections were

Table 1. Crystal Data

compound	K-1	K-2
formula	DyGeH <sub>8</sub> K <sub>5</sub> O <sub>43</sub> W <sub>11</sub>	ErGeH <sub>8</sub> K <sub>5</sub> O <sub>42</sub> W <sub>11</sub>
formula weight	3149.00	3135.75
crystal system	tetragonal	tetragonal
space group	<i>I4/m</i>	<i>I4/m</i>
<i>a</i> /Å	14.480(2)	14.4847(11)
<i>c</i> /Å	12.391(3)	12.3555(7)
<i>V</i> /Å <sup>3</sup>	2598.2(9)	2592.3(4)
<i>Z</i>	2	2
<i>T</i> /K	180(2)	180(2)
<i>F</i> (000)	2718	2664
<i>D<sub>c</sub></i> /Mg m <sup>-3</sup>	4.025	4.017
$\mu$ (Mo $K\alpha$ )/mm <sup>-1</sup>	26.713	26.868
data measured	9883	8968
unique data	1285	1285
<i>R</i> <sub>int</sub>	0.1134	0.1038
data with <i>I</i> ≥ 2σ( <i>I</i> )	949	1025
w <i>R</i> <sub>2</sub> (all data)	0.1340	0.1320
<i>S</i> (all data)	1.030	1.116
<i>R</i> <sub>1</sub> [ <i>I</i> ≥ 2σ( <i>I</i> )]	0.0459	0.0450
parameters/restraints	91/0	100/16
biggest diff. peak/hole/eÅ <sup>-3</sup>	+2.65/−1.43	+3.13/−0.97
CSD number	1908052	1908053

applied using XPREP in SHELXTL.<sup>101</sup> Structure solution was analyzed by dual-space direct methods (SHELXT),<sup>101</sup> followed by full-matrix least-squares refinement (SHELX-2016).<sup>102</sup> As is often the case in such Keggin structures, the central Ge(1) occupies a site of *I4/m* symmetry and appears to be bonded to eight symmetry-equivalent oxygens as a result, although a given Ge in the crystal is only bonded to four oxygens. O(1) was therefore refined with 50% occupancy. The single lanthanide cation in the cluster, Dy(2B) or Er(2B), was disordered against three W atoms W(2A) over four equivalent sites. In other words, the lanthanide cation, Dy(2B) or Er(2B), was, together with three W atoms, disordered over the four equivalent metal sites on the crystal mirror plane (Wyckoff 8h positions in *I4/m*). Atom O(6A), the tungstyl W = O oxygen bonded to W(2A), was thus refined with 75% occupancy. Electron density corresponding to four aqua ligands coordinated to Dy(2B) could be identified and refined with 25% occupancy. In K-2, one of these waters (and its symmetry equivalent) had a rather high thermal parameter and was refined as 12.5% occupancy;

each Er probably has three rather than four aqua ligands in the structure. The aqua ligands proved hard to refine, being at best oxygen atoms at a quarter occupancy. In addition to this, these ligands are disordered (in particular for the Er cluster, where three such ligands are disordered over the four sites), so that a more satisfactory refinement was not possible. No attempt was made to locate the H-atoms on these aqua ligands. Electron density in a cavity suggested the fifth (and badly disordered) K<sup>+</sup> cation, but attempts to refine it, or to model it using SQUEEZE, proved unsuccessful. Further details of the crystal structures investigation may be obtained from FIZ Karlsruhe, 76344 Eggenstein-Leopoldshafen, Germany (fax: (+49)7247-808-666; e-mail: crysdata@fiz-karlsruhe.de), on quoting the deposition number CSD-1908052 and CSD-1908053.

## ■ ASSOCIATED CONTENT

### Supporting Information

The Supporting Information is available free of charge at <https://pubs.acs.org/doi/10.1021/acsomega.9b02846>.

Crystallographic data in CIF format mi-21 (CIF)

Crystallographic data in CIF format 110912 (CIF)

Infrared spectra, thermograms, UV–vis spectra, emission spectra, and additional cyclic voltammograms for K-1 and K-2; table listing the peak assignment of K-1 observed during ESI MS (PDF)

## ■ AUTHOR INFORMATION

### Corresponding Author

\*E-mail: masooma.ibrahim@kit.edu.

### ORCID

Masooma Ibrahim: 0000-0002-8520-8585

Israël M. Mbomekallé: 0000-0003-3440-8066

Ananya Baksi: 0000-0003-3328-4399

Anthony B. Carter: 0000-0003-4641-6055

Christopher E. Anson: 0000-0001-7992-7797

### Author Contributions

All the authors contributed to this work. M.I. conceived and designed the experiments. M.I. characterized the compound and wrote the paper. Electrochemical studies were performed by I.M.M. and P.d.O. Mass spectrometry was carried out by A.B. Structure refinement were performed by A.B.C. and C.E.A. Y.P. processed the magnetic data. SEM studies were done by S.M. Elemental analyses were carried out by T.B. The manuscript was written with dedication of all authors. All authors have checked and approved the manuscript.

## Notes

The authors declare no competing financial interest.

## ACKNOWLEDGMENTS

M.I. thanks Prof. Annie K. Powell for continuous support and guidance. M.I. also thanks the University of Balochistan, Quetta, Pakistan, for allowing her to pursue her PhD and postdoctoral work at Jacobs University and KIT, respectively. M.I. and S.M. acknowledge support by the Helmholtz society through program Science and Technology of Nanosystems (STN). The authors acknowledge the networking support by the COST Actions MultiComp (CA15107) and MOLSPIN (CA15128), supported the COST Association (European Cooperation in Science and Technology). I.M.M. and P.d.O. thank the CNRS and the Université Paris-Sud for financial support. We also thank Sven Stahl and Eufemio Moreno-Pineda for performing thermogravimetric analysis measurements and (ac) magnetic susceptibility studies respectively. This work was partially carried out with the support of the Karlsruhe Nano Micro Facility (KNMF), a Helmholtz research infrastructure at Karlsruhe Institute of Technology.

## REFERENCES

- (1) Pope, M. T. *Heteropoly and Isopoly Oxometalates*; Springer: Berlin, 1983.
- (2) Long, D. L.; Tsunashima, R.; Cronin, L. Polyoxometalates: Building blocks for functional nanoscale systems. *Angew. Chem., Int. Ed.* **2010**, *49*, 1736–1758.
- (3) Vonci, M.; Boskovic, C. Polyoxometalate-supported lanthanoid single-molecule magnets. *Aust. J. Chem.* **2014**, *67*, 1542–1552.
- (4) Yamase, T. Photo- and electrochromism of polyoxometalates and related materials. *Chem. Rev.* **1998**, *98*, 307–325.
- (5) Ma, P.; Hu, F.; Wang, J.; Niu, J. Carboxylate covalently modified polyoxometalates: From synthesis, structural diversity to applications. *Coord. Chem. Rev.* **2019**, *378*, 281–309.
- (6) Chen, L.; Chen, W.; Wang, X.-L.; Li, Y.-G.; Su, Z.-M.; Wang, E.-B. Polyoxometalates in dye-sensitized solar cells. *Chem. Soc. Rev.* **2019**, *48*, 260–284.
- (7) Gao, P.; Wu, Y.; Wu, L. Co-assembly of polyoxometalates and peptides towards biological applications. *Soft Matter* **2016**, *12*, 8464–8479.
- (8) Du, D. Y.; Qin, J. S.; Li, S. L.; Su, Z. M.; Lan, Y. Q. Recent advances in porous polyoxometalate-based metal-organic framework materials. *Chem. Soc. Rev.* **2014**, *43*, 4615–4632.
- (9) Ma, X.; Yang, W.; Chen, L.; Zhao, J. Significant developments in rare-earth-containing polyoxometalate chemistry: Synthetic strategies, structural diversities and correlative properties. *CrystEngComm* **2015**, *17*, 8175–8197.
- (10) Boskovic, C. Rare earth polyoxometalates. *Acc. Chem. Res.* **2017**, *50*, 2205–2214.
- (11) Miras, H. N.; Vilà-Nadal, L.; Cronin, L. Polyoxometalate based open-frameworks (POM-OFs). *Chem. Soc. Rev.* **2014**, *43*, 5679–5699.
- (12) Passadis, S.; Kabanos, T. A.; Song, Y. F.; Miras, H. N. Self-assembly in polyoxometalate and metal coordination-based systems: Synthetic approaches and developments. *Inorganics* **2018**, *6*, 1–25.
- (13) Clemente-Juan, J. M.; Coronado, E.; Gaita-Ariño, A. Magnetic polyoxometalates: From molecular magnetism to molecular spintronics and quantum computing. *Chem. Soc. Rev.* **2012**, *41*, 7464–7478.
- (14) Chen, W.; Jiao, C.; Wang, X.; Shao, K.; Su, Z. Self-assembly of nanoscale lanthanoid-containing selenotungstates: Synthesis, structures, and magnetic studies. *Inorg. Chem.* **2019**, *58*, 12895–12904.
- (15) Hou, Y.; Chai, D.; Li, B.; Pang, H.; Ma, H.; Wang, X.; Tan, L. Polyoxometalate-incorporated metallacalixarene@graphene composite electrodes for high-performance supercapacitors. *ACS Appl. Mater. Interfaces* **2019**, *11*, 20845–20853.
- (16) Chai, D.; Gómez-García, C. J.; Li, B.; Pang, H.; Ma, H.; Wang, X.; Tan, L. Polyoxometalate-based metal-organic frameworks for boosting electrochemical capacitor performance. *Chem. Eng. J.* **2019**, *373*, 587–597.
- (17) Oms, O.; Dolbecq, A.; Mialane, P. Diversity in structures and properties of 3d-incorporating polyoxotungstates. *Chem. Soc. Rev.* **2012**, *41*, 7497–7536.
- (18) Haider, A.; Ibrahim, M.; Bassil, B. S.; Carey, A. M.; Viet, A. N.; Xing, X.; Ayass, W. W.; Miñambres, J. F.; Liu, R.; Zhang, G.; Keita, B.; Mereacre, V.; Powell, A. K.; Balinski, K.; N'Diaye, A. T.; Küpper, K.; Chen, H.-Yi.; Stimming, U.; Körtz, U. Mixed-valent Mn<sub>16</sub>-containing heteropolyanions: Tuning of oxidation state and associated physicochemical properties. *Inorg. Chem.* **2016**, *55*, 2755–2764.
- (19) Ibrahim, M.; Haider, A.; Xiang, Y.; Bassil, B. S.; Carey, A. M.; Rullik, L.; Jameson, G. B.; Doungmene, F.; Mbomekallé, I. M.; De Oliveira, P.; Mereacre, V.; Kostakis, G. E.; Powell, A. K.; Körtz, U. Tetradecanuclear Iron(III)-oxo nanoclusters stabilized by trilacunary heteropolyanions. *Inorg. Chem.* **2015**, *54*, 6136–6146.
- (20) Bassil, B. S.; Ibrahim, M.; Al-Oweini, R.; Asano, M.; Wang, Z.; Van Tol, J.; Dalal, N. S.; Choi, K. Y.; Ngo Biboum, R.; Keita, B.; Nadjjo, L.; Körtz, U. A planar {Mn<sub>19</sub>(OH)<sub>12</sub>}<sup>26+</sup> unit incorporated in a 60-tungsto-6-silicate polyanion. *Angew. Chem., Int. Ed.* **2011**, *50*, 5961–5964.
- (21) Ibrahim, M.; Mal, S. S.; Bassil, B. S.; Banerjee, A.; Körtz, U. Yttrium (III)-containing tungstoantimonate(III) stabilized by tetrahedral WO<sub>4</sub><sup>2-</sup> Capping Unit, [(Y(α-SbW<sub>9</sub>O<sub>31</sub>(OH)<sub>2</sub>(CH<sub>3</sub>COO)-(H<sub>2</sub>O))<sub>3</sub>(WO<sub>4</sub>)]<sup>17-</sup>. *Inorg. Chem.* **2011**, *50*, 956–960.
- (22) Ibrahim, M.; Bassil, B.; Körtz, U. Synthesis and characterization of 8-yttrium(III)-containing 81-tungsto-8-arsenate(III), [Y<sub>8</sub>(CH<sub>3</sub>COO)(H<sub>2</sub>O)<sub>18</sub>(As<sub>2</sub>W<sub>19</sub>O<sub>68</sub>)<sub>4</sub>(W<sub>2</sub>O<sub>6</sub>)<sub>2</sub>(WO<sub>4</sub>)]<sup>43-</sup>. *Inorganics* **2015**, *3*, 267–278.
- (23) Granadeiro, C. M.; De Castro, B.; Balula, S. S.; Cunha-Silva, L. Lanthanopolyoxometalates: From the structure of polyanions to the design of functional materials. *Polyhedron* **2013**, *52*, 10–24.
- (24) Bassil, B. S.; Dickman, M. H.; Römer, I.; Von Der Kammer, B.; Körtz, U. The tungstogermanate [Ce<sub>20</sub>Ge<sub>10</sub>W<sub>100</sub>O<sub>376</sub>(OH)<sub>4</sub>(H<sub>2</sub>O)<sub>30</sub>]<sup>56-</sup>: A polyoxometalate containing 20 cerium(III) atoms. *Angew. Chem., Int. Ed.* **2007**, *46*, 6192–6195.
- (25) Körtz, U.; Müller, A.; van Slageren, J.; Schnack, J.; Dalal, N. S.; Dressel, M. Polyoxometalates: Fascinating structures, unique magnetic properties. *Coord. Chem. Rev.* **2009**, *253*, 2315–2327.
- (26) Zhao, J.; Li, Y.; Chen, L.; Yang, G. Research progress on polyoxometalate-based transition-metal–rare-earth heterometallic derived materials: Synthetic strategies, structural overview and functional applications. *Chem. Commun.* **2016**, *52*, 4418–4445.
- (27) Bassil, B. S.; Körtz, U. Recent advances in lanthanide-containing polyoxotungstates. *Z. Anorg. Allg. Chem.* **2010**, *636*, 2222–2231.
- (28) Reinoso, S. Heterometallic 3d-4f polyoxometalates: Still an incipient field. *Dalton Trans.* **2011**, *40*, 6610–6615.
- (29) Reinoso, S.; Galán-Mascarós, J. R.; Lezama, L. New type of heterometallic 3d-4f rhomblike core in weakly-like polyoxometalates. *Inorg. Chem.* **2011**, *50*, 9587–9593.
- (30) Ibrahim, M.; Mereacre, V.; Leblanc, N.; Wernsdorfer, W.; Anson, C. E.; Powell, A. K. Self-assembly of a giant tetrahedral 3d-4f single-molecule magnet within a polyoxometalate system. *Angew. Chem., Int. Ed.* **2015**, *54*, 15574–15578.
- (31) Yu, T.; Ma, H.; Zhang, C.; Pang, H.; Li, S.; Liu, H. A 3d–4f Heterometallic 3D POMOF based on lacunary Dawson polyoxometalates. *Dalton Trans.* **2013**, *42*, 16328–16333.
- (32) Huo, Y.; Chen, Y. C.; Wu, S. G.; Liu, J. L.; Jia, J. H.; Chen, W. B.; Wang, B. L.; Zhang, Y. Q.; Tong, M. L. Effect of bridging ligands on magnetic behavior in dinuclear dysprosium cores supported by polyoxometalates. *Inorg. Chem.* **2019**, *58*, 1301–1308.
- (33) Hussain, F.; Conrad, F.; Patzke, G. R. A gadolinium-bridged polytungstoarsenate(III) nanocluster: [Gd<sub>8</sub>As<sub>12</sub>W<sub>124</sub>O<sub>432</sub>(H<sub>2</sub>O)<sub>22</sub>]<sup>60-</sup>. *Angew. Chem., Int. Ed.* **2009**, *48*, 9088–9091.
- (34) Wassermann, K.; Dickman, M. H.; Pope, M. T. Self-assembly of supramolecular polyoxometalates: The compact, water-soluble

heteropolytungstate anion  $[\text{As}_{12}^{\text{III}}\text{Ce}_1^{\text{III}}6(\text{H}_2\text{O})_{36}\text{W}_{14}\text{O}_{52}]^{76-}$ . *Angew. Chem., Int. Ed.* **1997**, *109*, 1513–1516.

(35) Li, H.; Wu, H.; Wan, R.; Wang, Y.; Ma, P.; Li, S.; Wang, J.; Niu, J. Utilizing the adaptive precursor  $[\text{As}_2\text{W}_{19}\text{O}_{67}(\text{H}_2\text{O})]^{14-}$  to support three hexanuclear lanthanoid-based tungstoarsenate dimers. *Dalton Trans.* **2019**, *48*, 2813–2821.

(36) Wu, H.; Zhi, M.; Chen, C.; Zhu, Y.; Ma, P.; Wang, J.; Niu, J. Synthesis, characterization, and photoluminescence properties of three two-dimensional lanthanide-containing Dawson-type polyoxometalates. *Dalton Trans.* **2019**, *48*, 13850–13857.

(37) Wu, H.; Yan, B.; Li, H.; Singh, V.; Ma, P.; Niu, J.; Wang, J. Enhanced photostability luminescent properties of  $\text{Er}^{3+}$ -doped near-white-emitting  $\text{Dy}_x\text{Er}_{(1-x)}$ -POM derivatives. *Inorg. Chem.* **2018**, *57*, 7665–7675.

(38) Wei, J.; Yang, L.; Ma, P.; Wang, J.; Niu, J. A series of multi-dimensional lanthanide-containing peroxoisopolymolybdates. *Cryst. Growth Des.* **2013**, *13*, 3554–3560.

(39) Artetxe, B.; Reinoso, S.; San Felices, L.; Lezama, L.; Gutiérrez-Zorrilla, J. M.; García, J. A.; Galán-Mascarós, J. R.; Haider, A.; Kortz, U.; Vicent, C. Cation-directed dimeric versus tetrameric assemblies of lanthanide-stabilized dilacunar Keggin tungstogermanates. *Chem. - Eur. J.* **2014**, *20*, 12144–12156.

(40) Ma, P.; Hu, F.; Huo, Y.; Zhang, D.; Zhang, C.; Niu, J.; Wang, J. Magnetoluminescent bifunctional dysprosium-based phosphotungstates with synthesis and correlations between structures and properties. *Cryst. Growth Des.* **2017**, *17*, 1947–1956.

(41) Reinoso, S.; Giménez-Marqués, M.; Galán-Mascarós, J. R.; Vitoria, P.; Gutiérrez-Zorrilla, J. M. Giant crown-shaped polytungstate formed by self-assembly of  $\text{Ce}^{\text{III}}$ -stabilized dilacunar Keggin fragments. *Angew. Chem., Int. Ed.* **2010**, *49*, 8384–8388.

(42) Liu, J. C.; Han, Q.; Chen, L. J.; Zhao, J. W.; Streb, C.; Song, Y. F. Aggregation of giant cerium–bismuth tungstate clusters into a 3D porous framework with high proton conductivity. *Angew. Chem., Int. Ed.* **2018**, *57*, 8416–8420.

(43) Wang, W.; Izarova, N. V.; van Leusen, J.; Kögerler, P.  $\text{Ce}^{\text{III}}$ -functionalized polyoxotungstates: discrete vs extended architectures. *Cryst. Growth Des.* **2019**, *19*, 4860–4870.

(44) Xu, X.; Chen, Y.; Zhang, Y.; Liu, Y.; Chen, L.; Zhao, J. Rare-earth and antimony-oxo clusters simultaneously connecting antimonotungstates comprising divacant and tetravacant Keggin fragments. *Inorg. Chem.* **2019**, *58*, 11636–11648.

(45) An, H.; Han, Z.; Xu, T. Three-dimensional architectures based on lanthanide-substituted double-Keggin-type polyoxometalates and lanthanide cations or lanthanide-organic complexes. *Inorg. Chem.* **2010**, *49*, 11403–11414.

(46) AlDamen, M. A.; Clemente-Juan, J. M.; Coronado, E.; Martí-Gastaldo, C.; Gaita-Arino, A. Mononuclear lanthanide single-molecule magnets based on polyoxometalates. *J. Am. Chem. Soc.* **2008**, *130*, 8874–8875.

(47) Ritchie, C.; Baslon, V.; Moore, E. G.; Reber, C.; Boskovic, C. Sensitization of lanthanoid luminescence by organic and inorganic ligands in lanthanoid-organic-polyoxometalates. *Inorg. Chem.* **2012**, *51*, 1142–1151.

(48) Ritchie, C.; Moore, E. G.; Speldrich, M.; Kögerler, P.; Boskovic, C. Terbium polyoxometalate organic complexes: correlation of structure with luminescence properties. *Angew. Chem., Int. Ed.* **2010**, *49*, 7702–7705.

(49) Salomon, W.; Dolbecq, A.; Roch-marchal, C.; Paille, G.; Dessapt, R.; Mialane, P.; Serier-brault, H. A multifunctional dual-luminescent polyoxometalate @ metal-organic framework  $\text{EuW}_{10}$  @  $\text{UiO-67}$  composite as chemical probe and temperature sensor. *Front. Chem.* **2018**, *6*, 1–8.

(50) Feng, J.; Li, X.; Pei, F.; Sun, G.; Zhang, X.; Liu, M. An evaluation of gadolinium polyoxometalates as possible MRI contrast agent. *Magn. Reson. Imaging* **2002**, *20*, 407–412.

(51) Feng, J.; Sun, G.; Pei, F.; Liu, M. Comparison between  $\text{GdDTPA}$  and two gadolinium polyoxometalates as potential MRI contrast agents. *J. Inorg. Biochem.* **2002**, *92*, 193–199.

(52) Arab Fashapoyeh, M.; Mirzaei, M.; Eshtiagh-Hosseini, H.; Rajagopal, A.; Lechner, M.; Liu, R.; Streb, C. Photochemical and electrochemical hydrogen evolution reactivity of lanthanide-functionalized polyoxotungstates. *Chem. Commun.* **2018**, *54*, 10427–10430.

(53) Li, S.; Zhou, Y.; Peng, Q.; Wang, R.; Feng, X.; Liu, S.; Ma, X.; Ma, N.; Zhang, J.; Chang, Y.; et al. Controllable synthesis and catalytic performance of nanocrystals of rare-earth-polyoxometalates. *Inorg. Chem.* **2018**, *57*, 6624–6631.

(54) Suzuki, K.; Tang, F.; Kikukawa, Y.; Yamaguchi, K.; Mizuno, N. Visible-light-induced photoredox catalysis with a tetracerium-containing silicotungstate. *Angew. Chem., Int. Ed.* **2014**, *53*, 5356–5360.

(55) Suzuki, K.; Sugawa, M.; Kikukawa, Y.; Kamata, K.; Yamaguchi, K.; Mizuno, N. Strategic design and refinement of Lewis acid-base catalysis by rare-earth-metal-containing polyoxometalates. *Inorg. Chem.* **2012**, *51*, 6953–6961.

(56) Boglio, C.; Lemièrre, G.; Hasenknopf, B.; Thorimbert, S.; Lacôte, E.; Malacria, M. lanthanide complexes of the monovacant Dawson polyoxotungstate  $[\alpha_1\text{-P}_2\text{W}_{17}\text{O}_{61}]^{10-}$  as selective and recoverable Lewis acid catalysts. *Angew. Chem., Int. Ed.* **2006**, *45*, 3324–3327.

(57) Dupré, N.; Rémy, P.; Micoine, K.; Boglio, C.; Thorimbert, S.; Lacôte, E.; Hasenknopf, B.; Malacria, M. Chemoselective catalysis with organosoluble Lewis acidic polyoxotungstates. *Chem. - Eur. J.* **2010**, *16*, 7256–7264.

(58) El Moll, H.; Nohra, B.; Mialane, P.; Marrot, J.; Dupré, N.; Riffade, B.; Malacria, M.; Thorimbert, S.; Hasenknopf, B.; Lacôte, E.; et al. Lanthanide polyoxocationic complexes: Experimental and theoretical stability studies and Lewis acid catalysis. *Chem. - Eur. J.* **2011**, *17*, 14129–14138.

(59) Peacock, R. D.; Weakley, T. J. R. Heteropolytungstate complexes of the lanthanide elements. Part I. Preparation and reactions. *J. Chem. Soc., A* **1971**, No. 1836.

(60) Wang, J. P.; Yan, Q. X.; Du, X.; Di, Niu, J. Y. Synthesis, crystal structure and characterization of two rare earth substituted Keggin-type germanotungstates. *Chin. J. Chem.* **2008**, *26*, 1239–1243.

(61) Mialane, P.; Lisnard, L.; Mallard, A.; Marrot, J.; Antic-Fidancev, E.; Aschehoug, P.; Vivien, D.; Sécheresse, F. Solid-state and solution studies of  $\{\text{Ln}_n(\text{SiW}_{11}\text{O}_{39})\}$  polyoxoanions: An example of building block condensation dependent on the nature of the rare earth. *Inorg. Chem.* **2003**, *42*, 2102–2108.

(62) Granadeiro, C. M.; De Castro, B.; Balula, S. S.; Cunha-Silva, L. Lanthanopolyoxometalates: From the structure of polyanions to the design of functional materials. *Polyhedron* **2013**, *52*, 10–24.

(63) Wang, J. P.; Duan, X. Y.; Du, X. D.; Niu, J. Y. Novel rare earth germanotungstates and organic hybrid derivatives: Synthesis and structures of  $\text{M}/[\alpha\text{-GeW}_{11}\text{O}_{39}]$  ( $\text{M} = \text{Nd}, \text{Sm}, \text{Y}, \text{Yb}$ ) and  $\text{Sm}/[\alpha\text{-GeW}_{11}\text{O}_{39}]$  (DMSO). *Cryst. Growth Des.* **2006**, *6*, 2266–2270.

(64) Naruke, H.; Iijima, J.; Sanji, T. Enantioselective resolutions and circular dichroism studies of lanthanide-containing Keggin-type  $[\text{Ln}(\text{PW}_{11}\text{O}_{39})_2]^{11-}$  Polyoxometalates. *Inorg. Chem.* **2011**, *50*, 7535–7539.

(65) Niu, J. Y.; Zhao, J. W.; Wang, J. P. Synthesis, crystal structure and characterization of a praseodymium<sup>III</sup>-substituted silicotungstate with a novel 1D chain connection motif. *Inorg. Chem. Commun.* **2004**, *7*, 876–879.

(66) Sadakane, M.; Dickman, M. H.; Pope, M. T. Controlled assembly of polyoxometalate chains from lacunary building blocks and lanthanide-cation linkers. *Angew. Chem.* **2000**, *39*, 2914–2916.

(67) Haraguchi, N.; Okaue, Y.; Isobe, T.; Matsuda, Y. Stabilization of tetravalent cerium upon coordination of unsaturated heteropolytungstate anions. *Inorg. Chem.* **1994**, *33*, 1015–1020.

(68) Bassil, B. S.; Dickman, M. H.; Von Der Kammer, B.; Kortz, U. The monolanthanide-containing silicotungstates  $[\text{Ln}(\beta_2\text{-SiW}_{11}\text{O}_{39})_2]^{13-}$  ( $\text{Ln} = \text{La}, \text{Ce}, \text{Sm}, \text{Eu}, \text{Gd}, \text{Tb}, \text{Yb}, \text{Lu}$ ): A synthetic and structural investigation. *Inorg. Chem.* **2007**, *46*, 2452–2458.

(69) Zheng, L.; Ying, M.; Zhang, G.; Yao, J.; Bassil, B. S.; Kortz, U.; Keita, B.; De Oliveira, P.; Nadjo, L.; Craescu, C. T.; et al. Molecular interaction between a gadolinium-polyoxometalate and human serum albumin. *Eur. J. Inorg. Chem.* **2009**, 5189–5193.

- (70) Luo, J.; Zhao, J.; Yuan, J.; Li, Y.; Chen, L.; Ma, P.; Wang, J.; Niu, J. An organic-inorganic hybrid 1-D double-chain copper-yttrium heterometallic silicotungstate  $[\text{Cu}(\text{Dap})_2(\text{H}_2\text{O})]_2\{\text{Cu}(\text{Dap})_2[\alpha\text{-H}_2\text{SiW}_{11}\text{O}_{39}\text{Y}(\text{H}_2\text{O})_2]\}_2 \cdot 10\text{H}_2\text{O}$ . *Inorg. Chem. Commun.* **2013**, *27*, 13–17.
- (71) Zhao, J.; Luo, J.; Chen, L.; Yuan, J.; Li, H.; Ma, P.; Wang, J.; Niu, J. Novel 1-D double-chain organic-inorganic hybrid polyoxotungstates constructed from dimeric copper-lanthanide heterometallic silicotungstate units. *CrystEngComm* **2012**, *14*, 7981–7993.
- (72) Zhao, H. Y.; Zhao, J. W.; Yang, B. F.; He, H.; Yang, G. Y. Organic-inorganic hybrids based on monovacant Keggin-type polyoxotungstates and 3d-4f heterometals. *CrystEngComm* **2013**, *15*, 8186–8194.
- (73) Zhao, J. W.; Li, Y. Z.; Ji, F.; Yuan, J.; Chen, L. J.; Yang, G. Y. Syntheses, structures and electrochemical properties of a class of 1-D double chain polyoxotungstate hybrids  $[\text{H}_2\text{Dap}][\text{Cu}(\text{Dap})_2]_{0.5}[\text{Cu}(\text{Dap})_2(\text{H}_2\text{O})][\text{Ln}(\text{H}_2\text{O})_3(\alpha\text{-GeW}_{11}\text{O}_{39})] \cdot 3\text{H}_2\text{O}$ . *Dalton Trans.* **2014**, *43*, 5694–5706.
- (74) Wang, X.; Liu, Y.; Jin, M.; Wu, Y.; Chen, L.; Zhao, J. W. Two families of rare-earth-substituted Dawson-type monomeric and dimeric phosphotungstates functionalized by carboxylic ligands. *Cryst. Growth Des.* **2017**, *17*, 5295–5308.
- (75) Wang, K.; Zhang, D.; Ma, J.; Ma, P.; Niu, J.; Wang, J. Three-dimensional lanthanide polyoxometalate organic complexes: Correlation of structure with properties. *CrystEngComm* **2012**, *14*, 3205–3212.
- (76) Zhou, W.; Zhang, Z.; Peng, J.; Wang, X.; Shi, Z.; Li, G. A series of hybrids with a framework constructed from  $\{-\text{SiW}_{11}\text{-Ln-SiW}_{11}\}_n$  chains and  $\{\text{Cu}/\text{Bimpy}\}$  ribbons. *CrystEngComm* **2014**, *16*, 10893–10901.
- (77) Zhao, H. Y.; Yang, B. F.; Yang, G. Y. Two new 2D organic-inorganic hybrids assembled by lanthanide-substituted polyoxotungstate dimers and copper-complex linkers. *Inorg. Chem. Commun.* **2017**, *84*, 212–216.
- (78) Zhao, H. Y.; Zhao, J. W.; Yang, B. F.; He, H.; Yang, G. Y. Novel organic-inorganic hybrid one-dimensional chain assembled by oxalate-bridging terbium-substituted phosphotungstate dimers and dinuclear copper(II)-oxalate clusters. *CrystEngComm* **2013**, *15*, 5209–5213.
- (79) Wang, J. P.; Zhao, J. W.; Duan, X. Y.; Niu, J. Y. Syntheses and structures of one- and two-dimensional organic-inorganic hybrid rare earth derivatives based on monovacant Keggin-type polyoxotungstates. *Cryst. Growth Des.* **2006**, *6*, 507–513.
- (80) Li, H.; Gong, P.; Jiang, J.; Li, Y.; Pang, J.; Chen, L.; Zhao, J. Organic-inorganic hybrids assembled from plenary Keggin-type germanotungstate units and 3d-4f heterometal clusters. *Dalton Trans.* **2019**, *48*, 3730–3742.
- (81) Martín-Caballero, J.; Artetxe, B.; Reinoso, S.; San Felices, L.; Vitoria, P.; Larrañaga, A.; Vilas, J. L.; Gutiérrez-Zorrilla, J. M. Thermostructural behavior in a series of lanthanide-containing polyoxotungstate hybrids with copper(II) complexes of the tetraazamacrocyclic cyclam: A single-crystal-to-single-crystal transformation study. *Inorg. Chem.* **2019**, *58*, 4365–4375.
- (82) Han, Q.; Wen, Y.; Liu, J.; Chen, L.; Zhao, J. Synthesis, structure and electrochemical properties of an inorganic-organic hybrid  $\text{Cu}^{\text{II}}\text{-Ce}^{\text{III}}$  heterometallic germanotungstate. *Inorg. Chem. Commun.* **2016**, *71*, 54–60.
- (83) Gong, P. J.; Pang, J. J.; Hu, H. F.; Li, H. J.; Chen, L. J.; Zhao, J. W. Ligand-controlled assembly of heteropolyoxomolybdates from plenary Keggin germanomolybdates and Cu-Ln heterometallic units. *Chem. - Asian J.* **2018**, *13*, 3762–3775.
- (84) Zhao, J.; Shi, D.; Chen, L.; Li, Y.; Ma, P.; Wang, J.; Niu, J. Novel polyoxometalate hybrids consisting of copper-lanthanide heterometallic/lanthanide germanotungstate fragments. *Dalton Trans.* **2012**, *41*, 10740–10751.
- (85) Qin, C.; Song, X. Z.; Su, S. Q.; Dang, S.; Feng, J.; Song, S. Y.; Hao, Z. M.; Zhang, H. J. New class of Preyssler-lanthanide complexes with modified and extended structures tuned by the lanthanide contraction effect. *Dalton Trans.* **2012**, *41*, 2399–2407.
- (86) Zhao, J. W.; Zheng, S. T.; Yang, G. Y. 0-D and 1-D inorganic-organic composite polyoxotungstates constructed from in situ generated monocopper<sup>II</sup>-substituted Keggin polyoxoanions and copper<sup>II</sup>-organoamine complexes. *J. Solid State Chem.* **2008**, *181*, 2205–2216.
- (87) von Allmen, K.; Morø, R.; Müller, R.; Soriano-lópez, J.; Linden, A.; Patzke, G. Nickel-containing Keggin-type polyoxometalates as hydrogen evolution catalysts: Photochemical structure-activity relationships. *ChemPlusChem* **2015**, *80*, 1389–1398.
- (88) Li, Y.; Xu, L.; Gao, G.; Jiang, N.; Liu, H.; Li, F.; Yang, Y. New fabrication of lanthanide complexes based on the polyoxometalate ligand of the  $[\alpha(1,4)\text{-GeW}_{10}\text{O}_{38}]^{12-}$  Anion. *CrystEngComm* **2009**, *938*, 1512–1514.
- (89) Bassil, B. S.; Kortz, U. Divacant polyoxotungstates: Reactivity of the gamma-decatungstates  $[\gamma\text{-XW}_{10}\text{O}_{36}]^{8-}$  (X = Si, Ge). *Dalton Trans.* **2011**, *40*, 9649–9661.
- (90) Wang, Y.; Xu, L.; Jiang, N.; Zhao, L.; Li, F.; Liu, X. Multidimensional frameworks constructed from Keggin-type heteropoly blue of molybdenum-tungsten cluster. *CrystEngComm* **2011**, *13*, 410–413.
- (91) Uchida, S.; Hashimoto, M.; Mizuno, N. A Breathing ionic crystal displaying selective binding of small alcohols and nitriles:  $\text{K}_3[\text{Cr}_3\text{O}(\text{OOCH})_6(\text{H}_2\text{O})_3][\text{A-SiW}_{12}\text{O}_{40}] \cdot 16\text{H}_2\text{O}$ . *Angew. Chem., Int. Ed.* **2002**, *6*, 2814–2817.
- (92) Kortz, U.; Ibrahim, M.; Dickman, M. H.; Suchopar, A. Large cation-anion materials based on trinuclear ruthenium(III) salts of Keggin and Wells-Dawson anions having water-filled channels. *Inorg. Chem.* **2009**, *48*, 1649–1654.
- (93) Ibrahim, M.; Moreno-pineda, E.; Bergfeldt, T.; Anson, C. E.; Powell, A. K. Synthesis and characterization of a heterometallic extended architecture based on a manganese (II)-substituted. *Materials* **2018**, *11*, No. 155.
- (94) Blasse, G.; Dirksen, G. J.; Zonneville, F. The luminescence of some lanthanide decatungstates and other polytungstates. *J. Inorg. Nucl. Chem.* **1981**, *43*, 2847–2853.
- (95) Keita, B.; Nadjo, L. Electrochemistry of Isopoly and Heteropoly Oxometalates. In *Encyclopedia of Electrochemistry*; Bard, A. J., Ed.; Wiley VCH, 2007.
- (96) Jing, J.; Burton-Pye, B. P.; Francesconi, L. C.; Antonio, M. R. Europium(III) reduction and speciation within a Wells-Dawson heteropolytungstate. *Inorg. Chem.* **2008**, *47*, 6889–6899.
- (97) Gupta, R.; Saini, M. K.; Doungmene, F.; De Oliveira, P.; Hussain, F. Lanthanoid containing phosphotungstates: The syntheses, crystal structure, electrochemistry, photoluminescence and magnetic properties. *Dalton Trans.* **2014**, *43*, 8290–8299.
- (98) Parent, L.; de Oliveira, P.; Teillout, A. L.; Dolbecq, A.; Haouas, M.; Cadot, E.; Mbomekallé, I. M. Synthesis and characterisation of the europium (III) dimolybdo-enneatungsto-silicate dimer,  $[\text{Eu}(\alpha\text{-SiW}_9\text{Mo}_2\text{O}_{39})_2]^{13-}$ . *Inorganics* **2015**, *3*, 341–354.
- (99) Keita, B.; Nadjo, L. Polyoxometalate-based homogeneous catalysis of electrode reactions: recent achievements. *J. Mol. Catal. A: Chem.* **2007**, *262*, 190–215.
- (100) Nsouli, N. H.; Bassil, B. S.; Dickman, M. H.; Kortz, U.; Keita, B.; Nadjo, L. Synthesis and structure of dilacunar decatungstogermanate,  $[\gamma\text{-GeW}_{10}\text{O}_{36}]^{8-}$ . *Inorg. Chem.* **2006**, *45*, 3858–3860.
- (101) Sheldrick, G. M. SHELXT—Integrated space-group and crystal-structure determination. *Acta Crystallogr., Sect. A: Found. Adv.* **2015**, *71*, 3–8.
- (102) Sheldrick, G. M. Crystal structure refinement with SHELXL. *Acta Crystallogr., Sect. C: Struct. Chem.* **2015**, *71*, 3–8.